

The Serendipitous XMM-Newton Cluster Athens Survey (SEXCLAS): Sample selection and the cluster $\log N - \log S$

V. Kolokotronis¹, A. Georgakakis¹, S. Basilakos¹, I. Georgantopoulos¹,
M. Plionis^{1,2}, S. Kitsionas^{1,4}, T. Gaga^{1,3}

¹ *Institute of Astronomy & Astrophysics, National Observatory of Athens, I.Metaxa & B.Pavlou, Palaia Penteli, 152 36, Athens, Greece*

² *Instituto Nacional de Astrofísica, Óptica y Electrónica (INAOE) Apartado Postal 51 y 216, 72000, Puebla, Pue., Mexico*

³ *Physics Department, Univ. of Athens, Panepistimioupolis, Zografou, Athens, Greece*

⁴ *Astrophysikalisches Institut Potsdam, An der Sternwarte 16, D-14482, Potsdam, Germany*

27 June 2018

ABSTRACT

In this paper we serendipitously identify X-ray cluster candidates using *XMM-Newton* archival observations complemented by 5-band optical photometric follow-up observations ($r \approx 23$ mag) as part of the X-ray Identification (XID) programme. Our sample covers an area of ≈ 2.1 deg² (15 *XMM-Newton* fields) and comprises a total of 21 (19 serendipitous + 2 target) extended X-ray sources to the limit $f_x(0.5 - 2 \text{ keV}) \approx 6 \times 10^{-15} \text{ erg s}^{-1} \text{ cm}^{-2}$, with a high probability (>99.9 %) of being extended on the *XMM-Newton* images. Of the 21 cluster candidates 7 are spectroscopically confirmed in the literature. Exploiting the optical data available for these fields we discover that $\gtrsim 68\%$ of the X-ray cluster candidates are associated with optical galaxy overdensities. We also attempt to constrain the redshifts of our cluster candidates using photometric methods. We thus construct the photometric redshift distribution of galaxies in the vicinity of each X-ray selected cluster candidate and search for statistically significant redshift peaks against that of the background distribution of field galaxies. Comparison of the photometric with spectroscopic redshift estimates for the confirmed clusters suggest that our simple method is robust out to $z \approx 0.5$. For clusters at higher- z , deeper optical data are required to estimate reliable photometric redshifts. Finally, using the sample of the 19 serendipitous X-ray selected cluster candidates we estimate their surface density down to $f_x(0.5 - 2 \text{ keV}) \approx 6 \times 10^{-15} \text{ erg s}^{-1} \text{ cm}^{-2}$ and find it to be in fair agreement with previous and recent studies.

Key words: Surveys: galaxies: clusters; Cosmology: large-scale structure of Universe; Surveys

1 INTRODUCTION

Since the first detection of the Virgo and Coma clusters at X-ray wavelengths (Byram, Chubb & Friedman 1966; Meekins et al. 1971), a large observational effort has been put forward aiming to compile X-ray cluster samples over a wide range of redshifts and luminosities. Such programs are mainly driven by the realisation that galaxy clusters, the most massive virialised systems known, are prime diagnostic tools for both cos-

mological models and structure formation theories (eg. Bahcall 1988; Borgani & Guzzo 2001; Rosati, Borgani & Norman 2002).

Eventhough the first all-sky cluster catalogues were carried out at optical wavelengths (Abell 1958; Zwicky et al. 1968; Abell, Corwin & Olowin 1989; Lumsden et al. 1992; Dalton et al. 1994), problems related to projection effects and complex selection criteria led to the search for alternative methods of compiling cluster samples. In this respect the X-ray wavelengths offer a crucial

feature: the X-ray emission of galaxy clusters is due to centrally concentrated hot gas that is relatively easy to identify against the X-ray sky. Therefore, X-ray selected samples are less prone to projection biases corrupting optical catalogues.

Several X-ray cluster samples have been accumulated and used for a variety of astrophysical and cosmological studies. The first all-sky X-ray cluster sample observed by *UHURU* contained 52 entries (Forman et al. 1978). This was followed by further X-ray missions, *Ariel-V* and *HEAO-1* that achieved even deeper observations (Cooke et al. 1978; Piccinotti et al. 1982). The launch of the *Einstein* Observatory, the first with imaging capabilities, provided a step forward in X-ray cluster astronomy. The *Einstein* Medium Sensitivity Survey covers almost 1000 deg² yielding a flux-limited sample of $\gtrsim 100$ clusters (Gioia et al. 1990; Henry et al. 1992). The advent of the *ROSAT* mission, with improved sensitivity and spatial resolution offered a further significant boost to cluster studies, providing samples over a wide range of depth, redshift and luminosity (Romer et al. 1994; Ebeling et al. 1996; 1998; 2001; Rosati et al. 1998; Vikhlinin et al. 1998; Romer et al. 2000; Böhringer et al. 2000; 2004; Perlman et al. 2002).

Recently, the *XMM-Newton* with 10 times more effective area and 5 times better spatial resolution than *ROSAT* provides an ideal platform to study clusters out to high- z (Pierre et al. 2004; Valtchanov et al. 2004). In addition to observational programs specifically designed to compile cluster samples (Pierre et al. 2004), the huge *XMM-Newton* public database also provides opportunities to perform serendipitous cluster surveys (Romer et al. 2001; Lamer et al. 2003; Basilakos et al. 2004 hereafter BPG04; Gaga et al. 2005 hereafter GPB05; Mullis et al. 2005). Land et al. (2005; hereafter LND05) for example, have combined public *XMM-Newton* observations with the Sloan Digital Sky Survey (SDSS; Abazajian 2003) and found that many of their extended X-ray sources are not associated with SDSS galaxy overdensities, indicating either high- z systems that require deeper optical data ($r > 22.5$) or groups of galaxies not standing out against the background. Furthermore, Plionis et al. (2005) using public *XMM-Newton* observations studied the X-ray properties of a subset of the Goto et al. (2002) optical SDSS clusters. They found that less than half of their 17 optically selected clusters have X-ray emission with a flux f_x (0.5 – 2 keV) $\gtrsim 1.2 \times 10^{-14}$ erg cm⁻² s⁻¹. The remaining SDSS clusters have a 3σ upper limit corresponding to $L_x \lesssim 5 \times 10^{42}$ erg/sec, implying very poor systems if real at all.

This paper presents first results from the ongoing Serendipitous X-ray Cluster Athens Survey (SEX-CLAS) using public *XMM-Newton* observations supplemented by 5-band optical photometry from the INT *XMM-Newton* Serendipitous Source Catalogue (SSC) XID program. In this first paper, we describe the selection of X-ray clusters, explore their association with optical galaxy overdensities, compare photometric with spectroscopic redshifts when possible and finally estimate their surface density. Compared to the LND05 study, our survey has somewhat deeper optical observations ($r \approx 23$) providing an advantage when study-

ing the association of X-ray clusters with optical galaxy overdensities. Additionally, we go a step further and estimate the $\log N - \log S$ of X-ray selected clusters. In what follows we employ a flat cosmology with $\Omega_\Lambda = 0.7$ and $H_0 = 100 h$ km s⁻¹ Mpc⁻¹.

2 OBSERVATIONS

2.1 Field selection

In this paper we use public *XMM-Newton* data with follow-up multiwaveband optical observations available as part of the *XMM-Newton* SSC XID programme. From a total of 77 *XMM-Newton* fields with optical photometric data available, we select those that (i) have imaging in at least 5 bands (U, g, r, i, z filters) to allow multi-color study of the cluster member galaxies, (ii) lie at high Galactic latitude $|b| > 20^\circ$ to avoid high hydrogen Galactic column densities and contamination by Galactic stars and (iii) have been observed by *XMM-Newton* with the EPIC-PN in full-frame mode. A total of 15 fields fulfill these criteria, 2 of which have clusters of galaxies as prime targets. Details on individual observations are presented in Table 1. Note that cluster targets are in fields #1 and #9.

2.2 X-ray data

The *XMM-Newton* data have been analysed using the Science Analysis Software (SAS 5.4.1). Event files for the PN and the two MOS detectors have been produced using the EPCHAIN and EMCHAIN tasks of SAS respectively. The event files were screened for high particle background periods by rejecting times with 0.5-10 keV count rates higher than 25 and 15 cts/s for the PN and the two MOS cameras respectively. The PN good time intervals for the fields used in this paper are shown in Table 1. Images in celestial coordinates with pixel size of 4.35'' have been extracted in the 0.5-2 keV spectral band for both the PN and the MOS event files. Exposure maps accounting for vignetting, CCD gaps and bad pixels have also been constructed.

2.3 Optical data

The optical data for this project have been obtained at the 2.5 m INT telescope using the Wide Field Camera (WFC) as part of the *XMM-Newton* SSC XID programme*. The WFC is mounted at the prime focus of the INT and comprises 4 thinned EEV 4kx2k CCDs with a pixel scale of 0.33''. The total sky coverage per exposure is 0.29 deg². The multiwaveband observations (U, g, r, i, z filters) are reduced using the pipeline reduction of the CASU INT Wide Field Survey[†], resulting in photometrically and astrometrically calibrated images. The exposure times are typically 10 min for the g, r filters and 40 min for U, i, z filters.

* <http://xmmssc-www.star.le.ac.uk/>

† www.ast.cam.ac.uk/~wfcSUR/

Table 1. Observing log of our survey. Columns are as follows: 1: index number, 2: XMM-Newton field name, 3, 4: equatorial coordinates of field center, 5: galactic latitude b (in degrees), 6: good time interval in ks.

Index number	Field name	α (J2000)	δ (J2000)	b (deg)	PN exp. time (ks)
1	CL 0016+16	00 18 40.3	+16 27 39.7	-45.71	25.6
2	Mrk 1014	01 59 43.5	+00 22 21.4	-57.94	4.8
3	SDS-1	02 17 53.5	-05 01 17.7	-59.75	40.2
4	SDS-2	02 19 29.6	-05 01 06.5	-59.49	37.8
5	GL 182	04 59 26.4	+01 46 04.9	-23.76	15.7
6	MS 0737.9+7441	07 44 34.8	+74 34 12.5	+29.57	27.0
7	PG 0844+349	08 47 31.5	+34 44 46.3	+37.96	7.3
8	Lockman Hole	10 52 29.1	+57 29 36.9	+53.14	33.7
9	MS 1137.5+6625	11 40 11.1	+66 10 24.2	+49.45	13.0
10	Mkn 205	12 22 10.1	+75 17 28.0	+41.67	10.7
11	HD 117555	13 30 38.2	+24 13 51.1	+80.68	33.0
12	PKS 2126-158	21 29 04.6	-15 39 59.9	-41.87	6.1
13	PKS 2135-147	21 37 38.5	-14 34 23.9	-43.33	30.0
14	IRAS 22491-18	22 51 42.6	-17 53 52.4	-60.95	15.9
15	EQ Peg	23 31 43.9	+19 54 43.1	-39.14	9.3

Source extraction and photometry is performed using the SExtractor package (Bertin & Arnouts 1996) with parameters (detection threshold and minimum area for detection) tuned to minimise the number of spurious detections, while ensuring that faint sources are included in the final catalogue. Regions contaminated by bright stars or bad pixels are masked during the source extraction. For the star-galaxy separation we have considered a size parameter, defined as the difference between the core, m_c , and ‘total’, m_t magnitude of sources in the r -band. The former corresponds to the intensity within an aperture with size similar to that of the seeing at the time of the observation and the latter is the Kron magnitude estimated by the SExtractor. As an example, Figure 1 plots the difference between the ‘total’ and ‘core’ magnitude (size parameter) against the ‘total’ magnitude in the case of a typical INT observation in the r -band (field #1 of Table 1). The stellar sequence is demarcated with a solid lined rectangular box. The distribution of stars and galaxies in Figure 1 overlaps at $r \geq 21$ mag. At fainter magnitudes no attempt is made to further eliminate stars from the sample, since compact galaxies could be mistakenly removed. Furthermore, the number of stars relative to galaxies becomes increasingly smaller beyond this magnitude. The r -band galaxy counts of a typical INT pointing (same as in Figure 1) are shown in Figure 2 along with the compilation of Metcalfe et al. (1991). At $r \leq 23$ mag, our results are in good agreement with the Metcalfe et al. (1991) number counts. At fainter magnitudes our sample is affected by incompleteness.

Moreover, we exploit the 5-band optical photometry in order to estimate photometric redshifts (z_p) for our sources using the HYPER-Z code (Bolzonella, Miralles & Pelló 2000). The HYPER-Z program determines the z_p of a given object by fitting a set of template Spectral Energy Distributions (SEDs) to the observed photometric data through a standard χ^2 minimisation technique. The template rest-frame SEDs used here are the observed mean spectra for four different galaxy types

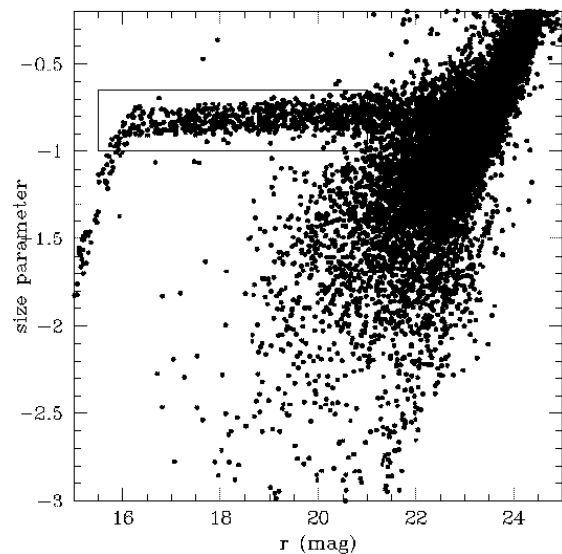


Figure 1. Star-galaxy separation diagram for the r -band data taken from field #1 of Table 1. The size parameter is defined as the difference between m_c and m_t (see text for details). The stellar sequence is demarcated by the solid line box.

(E/S0, Sbc, Scd, Im) from Coleman, Wu & Weedman (1980) extended in the UV and IR regions using the spectral synthesis models of Bruzual & Charlot (1993) with parameters selected to match the observed spectra.

Photometric redshifts are estimated only for those sources with at least 4-band (the 4 redder) photometric

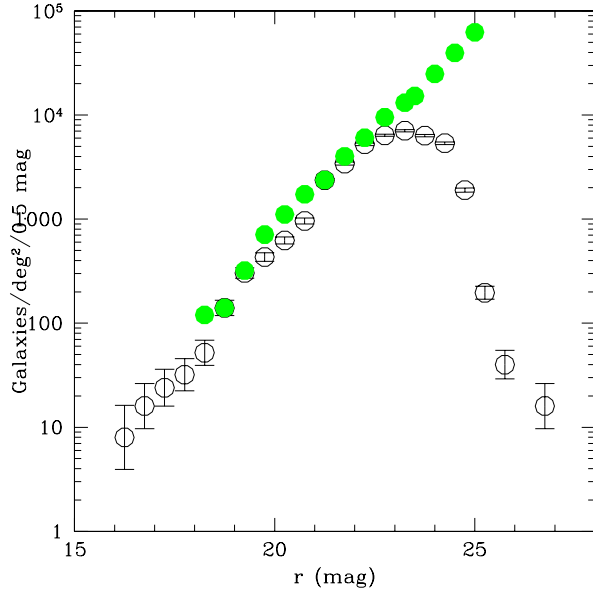


Figure 2. r -band galaxy counts of a typical INT observation (same as in Figure 1) used in this paper (open circles). The filled circles are the galaxy counts of Metcalfe et al. (1991).

information available. Comparison with spectroscopic redshifts found in the literature (NED) enables us to approximate the accuracy of our z_p which is thus computed via $\delta z_p / (1 + z_p) \approx 0.1$ and holds true for $z_p \leq 0.6$. This appears as an upper limit to the reliability of the estimated photometric redshifts of our X-ray selected clusters, which can be explained by the different limiting magnitudes of the 5 bands taken into account in the z_p estimates.

3 X-RAY CLUSTER SELECTION

The source detection is performed on the 0.5-2 keV PN image using the EWAVELET task of SAS with a 5σ detection threshold. We use the PN image due to the higher sensitivity of the EPIC-PN compared to the MOS detectors. A by-product of the source detection algorithm are smooth background maps providing an estimate of the background counts at each position. Cluster candidates are identified by searching for X-ray extended sources using the EMLDETECT task of SAS. This uses the EWAVELET source list as input and performs multi-PSF maximum likelihood fits to the count distribution of individual sources to assign a probability that an object is extended. We select clusters with EMLDETECT extension probability $> 99.9\%$. Visual inspection reveals that the choice of probability cutoff ensures that all obvious clusters are included in the catalogue while minimising the number of spurious detections. After excluding a total of 17 sources that clearly lie on CCD gaps or are related to double point sources, we finally extract a total of 21 cluster candidates with the above extension probability. These are presented in Table 2 together with their X-ray and optical properties.

Spectroscopic redshifts are available for 7 out of

the 21 cluster candidates, 2 of which are the prime targets of the respective XMM pointings (objects #2 and #16 in Table 2). For the remaining 14 X-ray selected cluster candidates there is no spectroscopic information available in the literature. The most distant cluster is at $z \sim 1.13$ (RX J1053.7+5735; Hashimoto et al. 2005), while the nearest lies at a $z = 0.386$ (VMF 98-021). A typical image of a spectroscopically identified X-ray cluster clearly associated with a nearby significant optical overdensity is shown in the right panel of Figure 3 (object #1 of Table 2).

For the flux estimation we use a circle with radius in the range $18''$ to $30''$ depending on the extent of the cluster on the *XMM-Newton* images. Count rates are converted to fluxes by choosing a Raymond-Smith model SED with temperature $T \approx 2$ keV and Galactic absorption appropriate for each field. We also apply a correction to the estimated fluxes to account for the cluster emission outside the aperture used to sum the source counts. We adopt a King’s surface brightness profile with core radius $r_c = 0.1 h^{-1}$ Mpc (Rosati et al. 1995; 1998) to estimate the flux fraction outside the aperture used. We convert radial apertures to physical coordinates using either the spectroscopic redshift (z_s) of the cluster (available for 7 systems) or z_p estimates described in section 4.2. In some cases there is no z_s or z_p and we assume $z = 0.4$, which coincides with the median expected redshift of the *ROSAT* deep cluster survey (Rosati et al. 1998). The corrected fluxes are presented in column 5 of Table 2.

We note that the EMLDETECT extended source identification algorithm produces reliable results when there is sufficient signal-to-noise ratio to perform multi-PSF maximum likelihood fits. It is therefore possible that high- z or intrinsically faint clusters with few photons may appear point-like on the *XMM-Newton* images and therefore missed from our sample. For example, Ostrander et al. (1998) searched for optical galaxy overdensities in the Hubble Space Telescope Medium Deep Survey and compiled a sample of optical cluster candidates. One of their systems, HST J001831+16207 (their Figure 5), overlaps with our survey (field #1) and coincides with an X-ray detected source classified as point-like by the EMLDETECT algorithm (see left panel of Figure 3). Limited spectroscopic information suggests an overdensity of optical galaxies at $z \approx 1.3$ (Yan & Thompson 2003; Yan et al. 2004) providing evidence that this might indeed be a real cluster.

4 OPTICAL IDENTIFICATION

In this section we exploit the 5-band optical photometry available for the surveyed area so as to study the optical properties of the X-ray selected cluster candidates. This is to search for optical galaxy overdensities, assess the reliability of our technique at least on spectroscopically identified systems (cf. right panel of Figure 3) and provide redshift estimates for those where spectroscopy is not available.

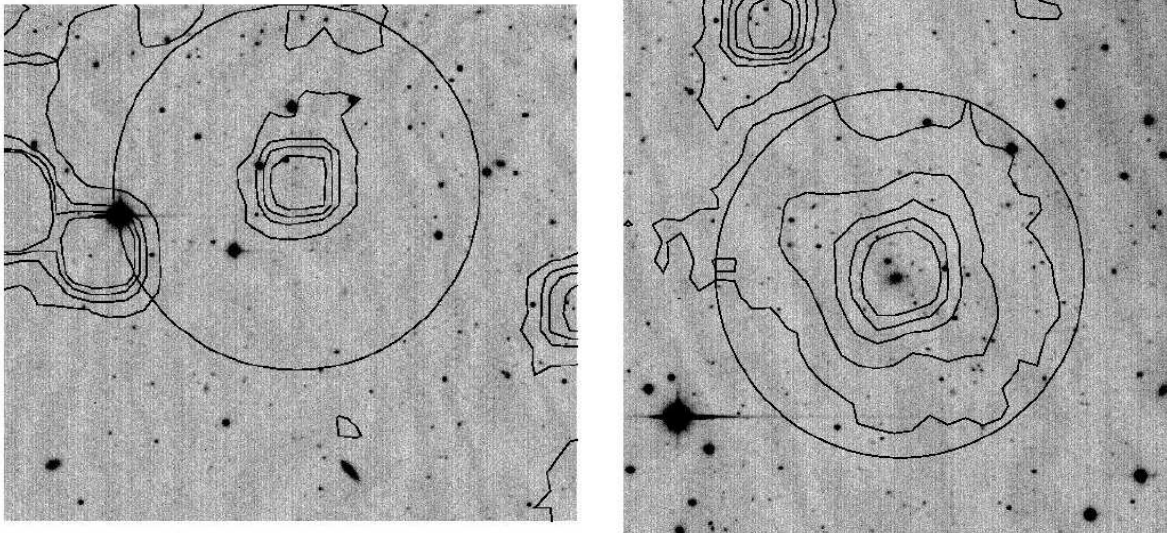


Figure 3. Underlying optical images versus X-ray gas contours for two distinct cases. **Left panel:** Distant cluster HST J001831+16207 (Ostrander et al. 1998) which appears as a point-like X-ray source in our survey. **Right panel:** A spectroscopically confirmed X-ray cluster associated with a nearby significant optical overdensity (object #1 of Table 2). In both panels, circles mark a $3'$ diameter.

4.1 Galaxy overdensities

We identify optical galaxy overdensities close to an X-ray selected cluster candidate using the smoothing and percolation technique described in detail by BPG04. Here we only briefly discuss the most salient details of the method. We smooth the projected galaxy population using a Gaussian kernel to produce continuous density maps. Following BPG04, we adopt a Gaussian kernel radius of $28.5''$ corresponding to $\sim 0.2 h^{-1}$ Mpc and a cell size of about $19''$ corresponding to $\sim 0.15 h^{-1}$ Mpc both at $z = 0.4$, the mean z_p of our optical data which is also comparable to the average redshift of the SDSS data reaching a similar but somewhat shallower depth (cf. Blanton et al. 2003). Clusters are identified on the resulting maps by searching for peaks above a projected overdensity of $\delta > 1$ and sizes larger than about $0.3 h^{-1}$ Mpc.

We exclude from the optical overdensity analysis objects #20 and #21 in Table 2 that lie within masked areas and hence have no optical data available. For the remaining cluster candidates, we apply the BPG04 technique to the optical data and identify projected optical galaxy overdensities in the vicinity of 13 out of 19 ($\gtrsim 68\%$) X-ray clusters, a finding also in broad agreement with recent analyses (Donahue et al. 2002; BPG04; Plionis et al. 2005). For the remaining 6 X-ray clusters, we do not find statistically significant optical overdensities insinuating either high- z systems that need deeper optical data or poor groups with few members. A further possibility could be that projection effects smear out possible optical overdensities. However, these may appear in the photometric distribution (object #13 in Table 2). Cluster candidates coupled with optical galaxy overdensities are presented in column 7 of Table 2.

It is interesting to mention that of the 7 previously

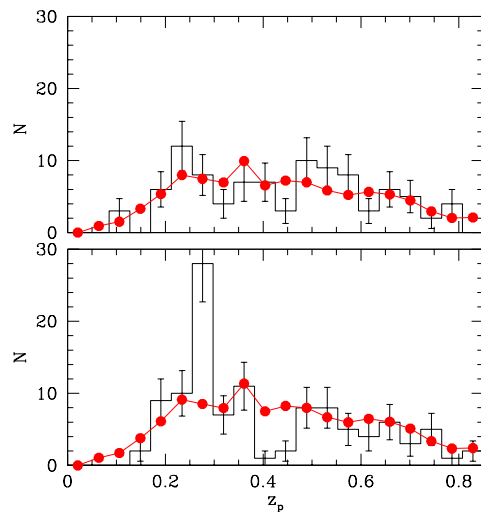


Figure 4. Photometric redshift distributions for two X-ray cluster candidates (histograms) over the total background z_p distribution (filled symbols). Poissonian errors are shown. Upper and lower panels correspond to clusters taken from fields #8 (object #14 of Table 2) and #15 (object #19 of Table 2), respectively.

known X-ray clusters, the BPG04 method has picked 6, the one missing being located within a masked region (object #20 of Table 2). We regard such a good performance as a measure of the technique's robustness.

4.2 Cluster photometric redshifts

In this section we use the z_p information in an attempt to constrain the redshifts of the X-ray selected cluster candidates. We construct the z_p distribution in the

Table 2. X-ray cluster candidates. The columns are: 1: index, 2: name from NED (if available), 3: right ascension α , 4: declination δ , 5: 0.5-2 keV flux, 6: 0.5-2 keV X-ray luminosity, 7: existence or not of an optical galaxy overdensity (δ_g), 8: Kolmogorov probability \mathcal{P}_K of significant peaks in the z_p distribution, 9: estimated photometric redshift, 10: spectroscopic redshift (if available) and 11: notes on individual objects. The latter includes usually target entries, distances from NED coordinates or even masked regions. The first 19 objects are located in *clean* areas and the last 2 fall entirely within masked areas of the optical image. Finally, entries with asterisks are also included in the X-ray cluster database BAX (<http://bax.ast.obs-mip.fr/>).

Index number	Cluster name	α (J2000)	δ (J2000)	f_x (10^{-14} cgs)	$\log L_x$	δ_g	\mathcal{P}_K	z_p	z_s	Notes
1	RX J0018.2+1617*	00 18 16.8	+16 17 39.8	4.05	43.69	✓	0.056	0.45	0.55	$\sim 8'$ from #2
2	MS 0015.9+1609*	00 18 33.4	+16 26 11.4	51.24	44.78	✓	0.0038	0.45	0.54	target
3	–	02 00 19.1	+00 19 33.2	3.01	43.48	✓	0.01	0.51	–	–
4	–	02 17 35.2	−05 13 26.0	1.17	–	✓	0.3	–	–	–
5	–	02 17 36.6	−04 59 24.7	0.66	–	✓	0.36	–	–	–
6	–	02 19 34.6	−05 08 57.0	2.47	–	×	0.483	–	–	–
7	–	02 19 44.6	−04 53 23.6	1.27	–	✓	0.154	–	–	–
8	–	02 19 44.8	−04 48 39.0	0.69	–	×	0.404	–	–	–
9	–	04 59 07.3	+01 54 47.7	2.22	–	×	0.73	–	–	–
10	–	08 47 02.2	+34 51 23.4	1.27	43.11	✓	0.0002	0.51	–	$\sim 3'$ from #11
11	VMF 98-059*	08 47 10.3	+34 48 57.6	3.88	43.69	✓	10^{-8}	0.52	0.56	0.37' from cluster
12	–	10 52 38.2	+57 30 49.3	0.8	43.10	✓	0.0004	0.61	–	$\sim 3'$ from #13
13	–	10 52 54.2	+57 32 09.6	0.62	42.93	×	0.0001	0.58	–	–
14	RX J1053.3+5719*	10 53 18.7	+57 20 38.0	2.57	43.00	✓	0.66	–	0.34	0.15' from cluster
15	RX J1053.7+5735*	10 53 40.3	+57 35 24.0	1.92	44.25	×	0.8	–	1.13	0.42' from cluster
16	MS 1137.5+6625*	11 40 23.0	+66 08 16.8	10.15	44.47	✓	0.1	0.36	0.782	target
17	–	21 36 59.5	−14 35 07.4	1.57	–	×	0.5	–	–	–
18	–	22 51 45.7	−18 05 38.4	1.20	–	✓	0.58	–	–	–
19	–	23 32 27.4	+19 58 04.8	4.74	43.03	✓	0.0016	0.27	–	–
20	VMF 98-021*	01 59 16.9	+00 30 07.2	26.7	44.15	×	–	–	0.386	mask & cluster
21	–	08 48 16.8	+34 36 09.0	3.14	–	×	–	–	–	mask

vicinity of a given X-ray selected cluster by extracting all galaxies within a $\sim 2.5'$ radius around the X-ray centroid. This search radius corresponds to a physical separation of $r_s \sim 0.85 h^{-1}$ Mpc at $z \sim 0.4$, the mean redshift of our photometric data. We then search for statistically significant peaks in the z_p distribution, implying the presence of a galaxy overdensity, by comparing with the mean photometric distribution of the galaxies in all the available fields. The background galaxy distribution is scaled to the number of galaxies extracted in the vicinity of the X-ray selected cluster.

We attempt to quantify the differences between the two distributions (background and generic cluster) using the Kolmogorov-Smirnov test to estimate the probability \mathcal{P}_K that they are drawn from the same parent population. A low probability may suggest the presence of galaxy overdensities, i.e. peaks in the distribution of galaxies in the vicinity of the X-ray selected cluster. We apply a cutoff in the probability $\mathcal{P}_K = 0.1$ to limit the sample with z_p estimates only to those clusters with statistically significant peaks against the background. We note, however, that there are X-ray cluster candidates with $\mathcal{P}_K > 0.1$, suggesting small differences between background and cluster distributions, where we can still identify peaks in the z_p distribution at the $\approx 2\sigma$ level (cf. objects #4, #5 of Table 2). This may hint at a group or a poor cluster with few members showing against the background distribution. Two examples of z_p distributions are presented in Figure 4. The upper plot (object #14 of Table 2) depicts a previously known X-ray clus-

ter with $\mathcal{P}_K > 0.1$, while the lower shows a prime X-ray cluster candidate as it is obvious from a visual look-over (object #19 of Table 2).

For clusters with $\mathcal{P}_K < 0.1$, the approximate z_p of a peak is firstly estimated via visual examination. In the case of many peaks we select the most statistically significant one on the basis of Poisson statistics. For a more accurate redshift estimate we adopt the method of LND05 and apply a Gaussian fit to the distribution in the vicinity of the visually identified statistically significant peak. The reduced χ^2 fits range between 1 and 2 and the probabilities of a good fitting are always ≥ 0.2 . The results are presented in column 9 of Table 2. For spectroscopically confirmed systems, despite the small number statistics, there is fair agreement between the spectroscopic and photometric cluster redshift estimates. The only exception is object #16 in Table 2 whose photometric distribution leads to a peak at $z_p \sim 0.36$, while $z_s = 0.782$ well beyond the point after which our z_p estimates are reliable (cf. section 2.3).

5 THE CLUSTER $\log N - \log S$

Using the cluster candidates presented in this paper we construct the $\log N - \log S$ for X-ray selected clusters. The survey sky coverage for extended sources is estimated by assuming a mean cluster size of $\sim 13''$ typical of the extent of our sources. A circular aperture with that radius is slid across the survey area to estimate at

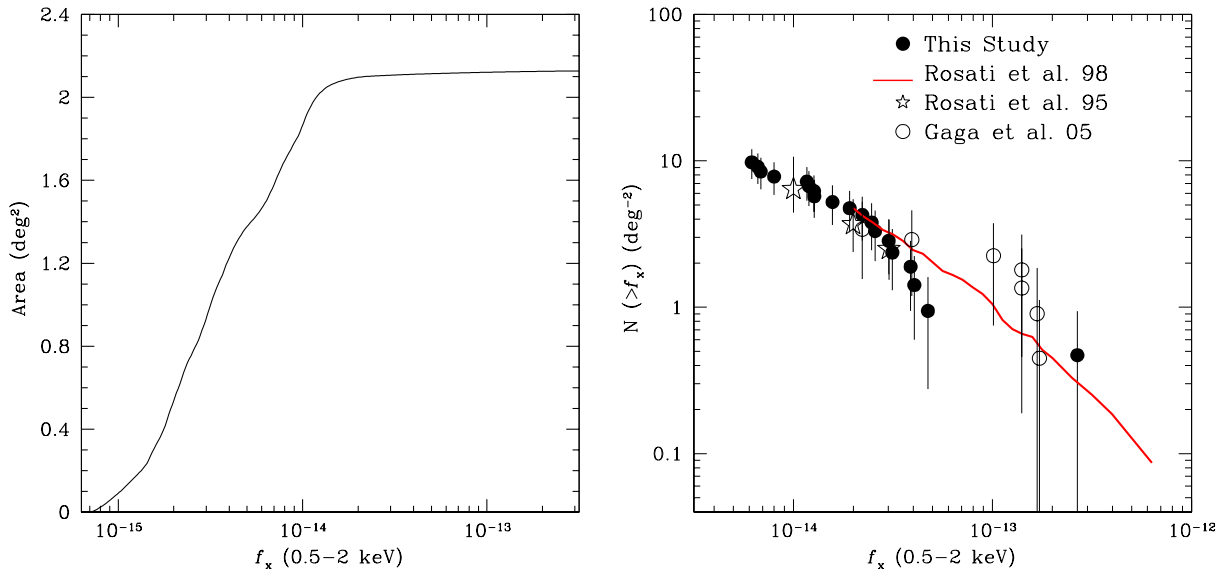


Figure 5. **Left panel:** Area curve for extended sources in our survey (see text for details). **Right panel:** Observed cluster cumulative number counts for the 19 serendipitous X-ray selected clusters in this paper (filled circles) compared to the cluster $\log N - \log S$ derived by Rosati et al. (1995; 1998) and that by GPB05. The errorbars are Poissonian estimates.

each position the 5σ fluctuations of the 0.5-2 keV background counts using the background maps, generated as a by-product of the source detection. These are then divided by the corresponding exposure time from the exposure map and converted to flux assuming a Raymond-Smith SED with temperature $T \sim 2$ keV and Galactic absorption appropriate for each field. We finally correct these fluxes for the emission outside the aperture used to sum the counts adopting a King’s surface brightness profile with $\beta = 0.7$ and $r_c = 0.1 h^{-1}$ Mpc (cf. GPB05). This procedure closely resembles our 5σ cluster detection and flux estimation methods applied to the *XMM-Newton* fields used in this paper and described in section 3.

The area curve measuring the solid angle available to an extended source of a given 0.5-2 keV flux is shown in the left plot of Figure 5. We note that this curve is not particularly sensitive to the choice of the aperture size used to sum the background counts, the SED adopted to convert count rates to fluxes or the correction factor to total flux. The X-ray cluster $\log N - \log S$ using the extended X-ray sources in our sample (with the exception of the two target clusters) is plotted in the right panel of Figure 5. The results of Rosati et al. (1995, 1998) using *ROSAT* PSPC data and those of GPB05 based on a serendipitous but shallower *XMM-Newton* survey are also shown. Our present survey nicely complements these studies reaching fainter flux limits. Moreover, there is a fair agreement between all the above samples within the 1σ uncertainties.

6 DISCUSSION AND CONCLUSIONS

We use a total of 15 public *XMM-Newton* pointings overlapping with 5-band optical data from the XID

programme to serendipitously identify X-ray selected clusters. In this first paper we present the selection of our cluster candidates, their optical properties, including their photometric and spectroscopic redshifts when available and their surface density to the limit $f_x(0.5 - 2 \text{ keV}) \approx 6 \times 10^{-15} \text{ erg s}^{-1} \text{ cm}^{-2}$.

We use the SAS packages to identify X-ray sources with high probability ($P > 99.9\%$) of being extended. After excluding spurious detections clearly associated with double X-ray point sources or falling on CCD gaps we identify a total of 21 bona-fide X-ray extended sources over a $\approx 2.1 \text{ deg}^2$ area which we call the SEX-CLAS sample. In this sample there are 7 spectroscopically confirmed clusters from the literature, 2 of which are *XMM-Newton* targets and hence not serendipitous sources.

We further exploit the optical multiwaveband data available for our fields to explore the optical properties of our sources and attempt to constrain their redshifts using photometric techniques. Firstly, we use the percolation technique described by BPG04 and identify galaxy overdensities in the vicinity of X-ray selected clusters for about 2/3 of our sources. This fraction is in fair agreement with previous studies on the optical properties of X-ray clusters using data reaching depths similar to those employed here ($r \approx 23 \text{ mag}$; BPG04; Plionis et al. 2005). The sources that are not linked with optical galaxy overdensities are either high- z clusters requiring deeper observations to be identified at optical wavelengths, or groups with too few members to stand out against the background/foreground galaxy surface density.

Next we attempt to use photometric techniques to estimate the redshifts of our cluster candidates. We construct the z_p distribution of all galaxies in the vicinity of X-ray selected clusters and compare it with that

of all optically selected galaxies from all 15 *XMM-Newton* pointings. Using the Kolmogorov-Smirnov statistical test we identify peaks in these distributions likely to be associated with the cluster candidates. For the spectroscopically confirmed clusters the agreement between z_p and z_s is good. We note however, that our method is insensitive to high- z clusters ($z > 0.5$) that lie beyond the magnitude limit of the existing optical data (Schuecker et al. 2004).

Finally, using our sample of 19 serendipitous cluster candidates (e.g. after excluding the two targets) we construct the *XMM-Newton* cluster $\log N - \log S$ to the limit $f_x (0.5 - 2 \text{ keV}) \approx 6 \times 10^{-15} \text{ erg s}^{-1} \text{ cm}^{-2}$. The estimated surface density is in fair agreement with previous *ROSAT* and recent *XMM-Newton* results. We note however, that the faint end in the right panel of Figure 5 might be affected by incompleteness due to high- z clusters with poor signal-to-noise ratio that does not allow reliable classification of their X-ray morphology (e.g. extended). There is at least one such example in our survey: a cluster at $z \approx 1.3$ that is paired with an X-ray source, albeit a point-like one. Deeper X-ray data are therefore demanded to probe thoroughly the $\log N - \log S$ for fluxes $\lesssim 5 \times 10^{-15} \text{ erg s}^{-1} \text{ cm}^{-2}$.

ACKNOWLEDGMENTS

This work is funded by the European Union and the Greek Ministry of Development in the framework of the Programme 'Competitiveness-Promotion of Excellence in Technological Development and Research-Action 3.3.1', Project 'X-ray Astrophysics with ESA's mission XMM', MIS-64564.

REFERENCES

- Abazajian K. et al. (The SDSS Collaboration), 2003, *AJ*, 126, 2081
- Abell G.O., 1958, *ApJS*, 3, 211
- Abell G.O., Corwin H.G., Olowin R.P., 1989, *ApJS*, 70, 1
- Bahcall N.A., 1988, *ARA&A*, 26, 631
- Basilakos S., Plionis M., Georgakakis A., Georgantopoulos I., Gaga T., Kolokotronis V., Stewart G.C., 2004, *MNRAS*, 351, 989 (BPG04)
- Bertin E., & Arnouts S., 1996, *A&AS*, 117, 393
- Blanton M. R. et al., 2003, *ApJ*, 592, 819
- Böhringer H., et al., 2000, *ApJS*, 129, 434
- Böhringer H., et al., 2004, *A&A*, *in press*
- Bolzonella M., Miralles J.-M., Pelló R., *A&A*, 363, 476
- Borgani, S., & Guzzo, L., 2001, *Nature*, 409, 39
- Bruzual A. G., & Charlot S., 1993, *ApJ*, 405, 538
- Byram E. T., Chubb T. A., Friedman H., 1966, *Science*, 152, 66
- Coleman G. D., Wu C. C., Weedman D. W., 1980, *ApJS*, 43, 393
- Cooke B. A. et al., *MNRAS*, 1978, 182, 489
- Dalton G. B., Efstathiou G., Maddox S. J., Sutherland W. J., 1994, *MNRAS*, 269, 151
- Donahue M., et al., 2002, *ApJ*, 569, 689
- Ebeling H., Voges W., Böhringer H., Edge A. C., Huchra J. P., Briel U. G., 1996, *MNRAS*, 281, 799
- Ebeling H. et al., 1998, *MNRAS*, 301, 881
- Ebeling H., Edge A. C., Henry J. P., 2001, *ApJ*, 553, 668
- Forman W. et al., 1978, *ApJS*, 38, 357
- Gaga T., Plionis M., Basilakos S., Georgantopoulos I., Georgakakis A., 2005, *submitted* (GPB05)
- Gioia I., Henry J., Maccacaro T., Morris S., Stocke J., Wolter A., 1990, *ApJ*, 356, L35
- Goto T. et al., 2002, *AJ*, 123, 1807
- Hashimoto Y., Henry J. P., Hasinger G., Szokoly G., Schmidt M., Lehmann I., 2005, *A&A*, *accepted*, astro-ph/0502482
- Henry J., Gioia I., Maccacaro T., Morris S., Stocke J., Wolter A., 1992, *ApJ*, 386, 408
- Lamer G., Schwobe A., Elvis M., Burke D., Watson M., 2003, *AN*, 324, 156
- Land K. et al., 2005, astro-ph/0405225 (LND05)
- Lumsden S. L., Nichol R. C., Collins C. A., Guzzo L., 1992, *MNRAS*, 258, 1
- Meekins J. F., Gilbert F., Chubb T. A., Friedman H., Henry R. C., 1971, *Nature*, 231, 107
- Metcalfe N., Shanks T., Fong R., Jones L. R., 1991, *MNRAS*, 249, 498
- Mullis C. R., Rosati P., Lamer G., Böhringer H., Schwobe A., Schuecker P., Fassbender R., 2005, *ApJL*, *accepted*, astro-ph/0503004
- Ostrander E. J., Nichol R. C., Ratnatunga K. U., Griffiths R. E., 1998, *AJ*, 116, 2644
- Perlman E. S., Horner D. J., Jones L. R., Scharf C. A., Ebeling H., Wegner G., Malkan M., 2002, *ApJS*, 140, 265
- Piccinotti G. et al., 1982, *ApJ*, 253, 485
- Pierre M. et al., 2004, *A&A*, *submitted*
- Plionis M., Basilakos S., Georgantopoulos I., Georgakakis A., 2005, *ApJL*, *in press*, astro-ph/0410293
- Romer K. et al., 1994, *Nature*, 372, 75
- Romer K. et al., 2000, *ApJS*, 126, 209
- Romer K., Viana P., Liddle A., Mann R., 2001, *ApJ*, 547, 594
- Rosati P., Della Ceca R., Burg R., Norman C., Giacconi R., 1995, *ApJ*, 445, L11
- Rosati P., Della Ceca R., Norman C., Giacconi R., 1998, *ApJ*, 492, L21
- Rosati P., Borgani S., Norman C., 2002, *ARA&A*, 40, 539
- Schuecker P., Böhringer H., Voges W., 2004, *A&A*, 420, 61
- Valtchanov I. et al., 2004, *A&A*, 423, 75
- Vikhlinin A., McNamara B., Forman W., Jones C., Quintana H., Hornstrup A., 1998, *ApJ*, 502, 558
- Yan L., & Thompson D., 2003, *ApJ*, 586, 765
- Yan L., Thompson D., Soifer B. T., 2004, *AJ*, 127, 1274
- Zwicky, F., Herzog, E., Wild, P., 1968, Pasadena: California Institute of Technology (CIT), 1961-1968